Exploring the mixed transport properties of sulfur (VI)-doped Ba2In2O5 for intermediate-temperature electrochemical applications

Pérez-Flores, Juan Carlos ; Nasani, Narendar ; Perez-Coll, D; Slater, Peter; Fagg, Duncan

DOI:
10.1039/C6TA02708C

Document Version
Peer reviewed version

Citation for published version (Harvard):
Pérez-Flores, JC, Nasani, N, Perez-Coll, D, Slater, P & Fagg, D 2016, 'Exploring the mixed transport properties of sulfur (VI)-doped Ba2In2O5 for intermediate-temperature electrochemical applications', *Journal of Materials Chemistry A*. https://doi.org/10.1039/C6TA02708C

Journal of
Materials Chemistry A

Accepted Manuscript

This article can be cited before page numbers have been issued, to do this please use: D. Pérez-Coll, J. C. Pérez Flores, N. narendar, P. Slater and D. P. fagg, *J. Mater. Chem. A*, 2016, DOI: 10.1039/C6TA02708C.

This is an *Accepted Manuscript*, which has been through the Royal Society of Chemistry peer review process and has been accepted for publication.

Accepted Manuscripts are published online shortly after acceptance, before technical editing, formatting and proof reading. Using this free service, authors can make their results available to the community, in citable form, before we publish the edited article. We will replace this *Accepted Manuscript* with the edited and formatted *Advance Article* as soon as it is available.

You can find more information about *Accepted Manuscripts* in the Information for Authors.

Please note that technical editing may introduce minor changes to the text and/or graphics, which may alter content. The journal's standard Terms & Conditions and the Ethical guidelines still apply. In no event shall the Royal Society of Chemistry be held responsible for any errors or omissions in this *Accepted Manuscript* or any consequences arising from the use of any information it contains.

ROYAL SOCIETY OF CHEMISTRY

www.rsc.org/materialsA

View Article Online
DOI: 10.1039/C6TA02708C

Journal Name

ARTICLE

Exploring the mixed transport properties of sulfur (VI)-doped $Ba_2In_2O_5$ for intermediate-temperature electrochemical applications

Received 00th January 20xx,
Accepted 00th January 20xx

DOI: 10.1039/x0xx00000x

www.rsc.org/

D. Pérez-Coll[a], Juan Carlos Pérez-Flores[b], Narendar Nasani[a], Peter R. Slater[c] and Duncan P. Fagg[a*]

Thestabilised orthorhombic perovskite $Ba_2In_{1.8}S_{0.2}O_{5.3}$ was synthesised by solid state reaction at low-temperature. The mixed (electronic-protonic-oxide-ionic) conducting properties of this composition were investigated in detail for potential interest in a wide range of membrane applications including Protonic Ceramic Fuel Cells. The electrochemical analyses performed include impedance spectroscopy in wet/dry conditions of N_2 and O_2 and modified electromotive force measurements in wet/dry mixtures of N_2/O_2. In dry oxidising conditions the sample possesses mixed electronic-oxide-ionic contributions to the electrical transport in the whole range of temperature, associated with the equilibrium between oxygen vacancies and holes. In wet atmospheres, protonic species arise from the hydration reaction. Protons represent the dominant charge carriers for temperatures lower than 550 °C, while oxide-ions and holes are the major mobile species for temperatures higher than 700 °C. Appreciable mixed contributions to the electrical transport from protons, oxide ions and holes are confirmed between 550-700 °C. The experimental data obtained from modified electromotive force measurements and impedance spectroscopy fit well with the expected results according to the proposed defect chemistry model.

1. Introduction

The search for ionic (both protonic and oxide-ionic) conductors with energy technological applications have attracted great attention due to their potential use as humidity and/or hydrogen/oxygen sensors, oxygen pumps, selective membranes and electrolytes in intermediate and high temperature solid oxide fuel cells (SOFCs) [1-4]. The present state-of-the-art, reference materials are those operating at high temperatures, mainly with fluorite-type structures (for example, CaO- or Y_2O_3-doped ZrO_2). Nonetheless, for operational use in devices of commercial relevance, restriction to temperatures below 600ºC has been suggested, due to enhanced cell longevities and reduced cost of balance of plant [5, 6]. The search for alternative materials that offer higher ionic conductivities at lower temperatures has, thus, become a highly active area of research to facilitate this transition. Perovskite-type and crystallographically related materials can offer this opportunity as they tolerate high compositional flexibility that permits the tailoring of properties by manipulation of defect chemistry.

In this context, $Ba_2In_2O_5$ was recognized to exhibit high oxide- and protonic-ion conductivity at elevated and intermediate temperatures, respectively[7-11]. The $Ba_2In_2O_5$ brownmillerite structure ($A_2B_2O_5$) can be described as a common perovskite (ABO_3) with 1/6 of oxygen vacancies sited along the direction of an orthorhombic symmetry[9]; resulting in ordered alternating sheets of [BO_6] octahedra and [BO_4] tetrahedra. At high temperature (≈ 925 °C), oxygen vacancies become randomly distributed leading to phase transition to cubic perovskite symmetry with high ionic conductivity[7, 12, 13]. In addition, a new and reversible phase transition from the α-form, $Ba_2In_2O_5$, to the β-phase, $Ba_2In_2O_5.H_2O$ (tetragonal symmetry, *P4/mmm*), was reported at temperatures around 300 ºC, under wet atmospheres. Although the β-phase is considered an excellent proton conductor, its use in electrochemical devices could not be recommended, due to substantial volume changes during the phase transition[12, 14, 15].

Following the objective to enhance the chemical and structural stability as well as the conductivity of $Ba_2In_2O_5$ at fuel cell operating conditions, several recent works proposed alternative dopant substitutions, either in the A-, B-site or both sites simultaneously. The main objective is to stabilize the high temperature phase, of oxygen vacancy disorder, to lower temperatures to promote high levels of proton or oxide-ion conductivity. Sr^{2+} substitution at the A-site was found to increase the order-disorder temperature transition (T_d) whereas Ga^{3+} substitution at B-site was shown to decreases it [16, 17]. The addition of lanthanum in $Ba_{2-x}La_xIn_2O_5$ lowered T_d until the disordered high temperature phase was finally stabilised to room temperature in compositions with values of

[a] Nanotechnology Research Division, Centre for Mechanical Technology and Automation, Department of Mechanical Engineering, University of Aveiro, 3810-193, Aveiro, Portugal. *Correspondence - duncan@ua.pt
[b] Chemistry Department, Facultad de Farmacia, Universidad CEU-San Pablo, Boadilla del Monte, Madrid 28668, Spain.
[c] School of Chemistry, University of Birmingham, Birmingham B15 2TT, UK.

View Article Online
DOI: 10.1039/C6TA02708C

x > 0.1[18, 19]. Examples of B-site aliovalent substitution can also be found. Substitution of In^{3+} by rare earth elements, $Ba_2In_{2-x}R_xO_5$ (being R = Sc, Lu, Yb, Gd, Sm,)[20, 21] produced a T_d temperature decrease for cations smaller than indium related to their preferential occupation of the tetrahedral [InO_4] sites instead of the octahedral positions[22]. B-site substitutions with Ce were shown to yield a proton conductor with significant conductivity in the 100-300ºC temperature range, generating a potential candidate even for fuel cells operating at very low temperatures[23]. More recently, new doping strategies based on oxyanion substitutions in B-site have attracted attention. SO_4^{2-}, PO_4^{3-} or SiO_4^{4-} anion[24-27] doping in the B-site favour anionic disorder and simultaneously increase the oxide-ion conductivity at lower temperatures and proton conductivity under humid conditions.

In the framework of such oxyanion doping, the present work explores the perovskite composition $Ba_2In_{1.8}S_{0.2}O_{5+\delta}$ obtained by the solid-state method. The formation of a single phase composition is verified by X-ray diffraction (XRD). Impedance spectroscopy (IS) is used to determine the electrical conductivity under different gas atmospheres. Moreover, more detailed conduction characteristics are analyzed by electromotive force (EMF) measurements under both dry and wet conditions. The contribution of either protonic- oxide-ionic and hole charge carriers to the total transport phenomenon at different pO_2, pH_2O and T, linked to the defect chemistry interpretation, allows the applicability of $Ba_2In_{2-x}S_xO_{5+\delta}$ as an active material in intermediate temperature SOFCs and other electrochemical devices to be assessed.

2. Experimental Procedure

$Ba_2In_{1.8}S_{0.2}O_{5.3}$ was prepared by solid-state reaction in a similar process to that previously described[24]. Stoichiometric amounts of high purity reagents, $BaCO_3$ (Aldrich, 99.98%), In_2O_3 (Aldrich, 99.99%) and $(NH_4)_2SO_4$ (Fluka, >98%) were weighed and, subsequently mixed in a mortar and pestle; a 3% excess of $BaCO_3$ was added to compensate for possible Ba losses under high temperature sintering[28]. The sample was then pelletized, heated at 1000 °C for 12 h (5 °C min^{-1} ramp rate) and cooled down to room temperature (RT). After crushing and homogenization, resulting powders were ball-milled at 250 rpm for 2 h (planetary ball mill PM200, Retsch) using ZrO_2 vessel and balls. Powders were again pelletized, heated at 1000 °C for 50 h and cooled down to RT (5 °C min^{-1} heating/cooling ramp rate).

The phase purity of the pale yellow colour samples obtained was analyzed by powder X-ray diffraction (XRD) using Bruker D8 high-resolution diffractometer equipped with a position sensitive detector (PSD) MBraun PSD-50M, with a monochromatic $CuK_{\alpha1}$ (λ = 1.5406 Å) radiation obtained with a germanium primary monochromator. Diffraction patterns were analyzed by Lebail fitting using the FullProf software[29] in the 2θ = 10–140º angular range.

Scanning electron microscopy (SEM) were performed with a FEI XL30® system (4000 magnification) equipped with an EDAX® analyser for energy dispersive spectroscopy (EDS).

The experimental specimens for impedance spectroscopy (IS) were prepared by ball-milling (350 rpm for 1 h) the heated samples, isostatic pressing in cylindrical die (200 MPa, ≈12 mm diameter) and sintering at 1300 °C for 6 h (heating and cooling rates of 2 ºC min^{-1}) to yield pellets of ≈ 10 mm diameter and ≈ 2 mm thick. The as-obtained samples exhibited closed porosity and a relative density ~ 90 %. Platinum paste was painted on each side of the pellets and fired at 900 ºC for 2 h to yield the contact electrodes. IS measurements were performed with a PGSTAT302N Autolab (Ecochemie) by applying AC signal with an amplitude of 50 mV in the frequency range 0.1-10^6 Hz and measured in the direction of decreasing temperature over the 850-350°C temperature interval (50 °C $step^{-1}$). The experimental procedure was applied to dry/wet N_2 and O_2 atmospheres. Humid conditions were obtained by bubbling gases through room temperature KCl saturated distilled water in a thermostatic flask. Dry conditions were obtained using a Varian moisture gas clean filter. Repeated impedance measurements were recorded to confirm the equilibrium of the system. ZView software (Scribner Associates) was used to analyze the impedance spectra.

EMF measurements were carried out in a controlled atmosphere device similar to that previously described[30]. A sintered pellet of $Ba_2In_{1.8}S_{0.2}O_{5+\delta}$ was hermetically sealed onto a YSZ sensor tube which was introduced into a closed alumina tube. Each chamber of the cell was equilibrated in selected atmospheres by flowing different gas mixtures in the 500-800 ºC temperature range (50 °C $step^{-1}$). The oxidizing conditions of the gas mixtures were obtained by selecting different O_2/N_2 rates while various levels of humidity were achieved by mixing different proportions of wet and dry atmospheres[31]. To avoid the thermovoltage contribution, voltage measures were corrected by inverting the gas compositions present in each chamber (thereby, inverting the chemical potential gradient), allowing the offset potential to be eliminated from the measured voltages[31]. The effect of electrode polarization on the measured values of electromotive force of the system was taken into account by an active load modification of the methodology. For this purpose the electromotive force was monitored as a function of a variable external resistance located in parallel to the system, as previously reported[32, 33]. Voltage measurements were collected for different values of resistances using a Fluke 45 digital multimeter.

3. Results and discussion

3.1 Structural analysis

The X-ray powder diffraction pattern of $Ba_2In_{1.8}S_{0.2}O_{5+\delta}$ showed a pure phase material without any secondary phases. The pattern was fully indexed by LeBail refinement (Figure 1) in the orthorhombic system (S.G. *Icmm* #74) to give lattice parameters of *a* = 5.9739(2), *b* = 16.9978(6) and *c* = 6.0477(3) Å, which result in a cell volume of 614.10 $Å^3$, in close

View Article Online
DOI: 10.1039/C6TA02708C

agreement to that previously reported[25]. The current results, thereby, reinforce the work of Shin et al. [25] to show that introduction of sulfur in the $Ba_2In_2O_{5+\delta}$ structure promotes oxygen sublattice disorder and formation of the perovskite phase.

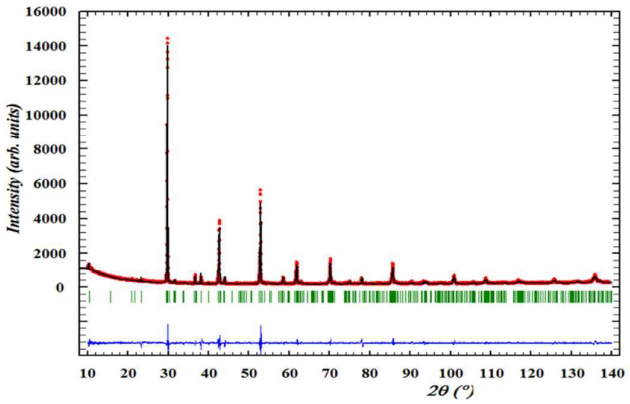

Figure 1. Observed (red points), calculated (solid black line) and difference (blue line at the bottom) patterns for the LeBail refinement of $Ba_2In_{1.8}S_{0.2}O_{5+\delta}$ diffraction pattern. The vertical green bars indicate the peak positions of all allowed Bragg reflections for *Icmm* S. G.

3.2 Microstructure

Figure 2 displays SEM analyses of the $Ba_2In_{1.8}S_{0.2}O_{5+\delta}$ ceramic pellet. The back-scattered electron (BSE) image in Fig. 2(a) suggests high homogeneity and no segregation or secondary phases, showing very uniform contrast colours. Energy Dispersive X-ray spectroscopy (EDS) confirms $Ba_2In_{1.8}S_{0.2}O_{5+\delta}$ as single phase and table 1 shows that the experimental chemical composition is in agreement to the expected nominal stoichiometry. The elemental distribution of EDS maps (Fig. 2(b-e)) show good sample homogeneity, reinforcing the absence of secondary phases.

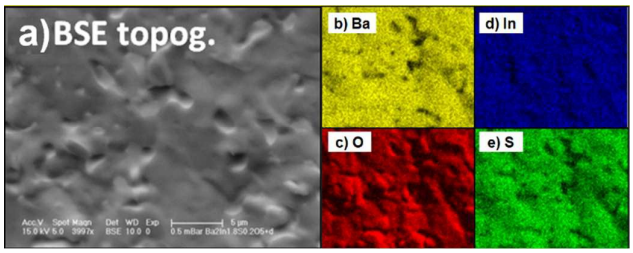

Figure 2. SEM micrographs of $Ba_2In_{1.8}S_{0.2}O_{5+\delta}$ at x4000 magnification factor: a) Back-scattered electrons (BSE) image and corresponding topographic view, and b), c), d) and e) correspond to Ba, O, In and S elemental distribution maps.

Table 1. Nominal and experimental chemical compositions (as determined by EDS) of $Ba_2In_{1.8}S_{0.2}O_{5+\delta}$.

Description	Nominal	Sintered sample
Ba / In	1.11	1.13(2)
In / S	9.00	8.50(2)
Ba / S	10.00	9.63(1)

3.3 Electrical transport properties of $Ba_2In_{1.8}S_{0.2}O_{5+\delta}$

The electrical conductivity of $Ba_2In_{1.8}S_{0.2}O_{5+\delta}$ was studied as a function of temperature in dry/wet N_2 and O_2 atmospheres by electrochemical impedance spectroscopy (IS) by deconvolution of the contributions ascribed to the bulk, grain boundary and electrode responses.

Figure 3 shows some examples of impedance spectra at 408 ºC for dry/wet O_2 and N_2, where substantial differences can be identified according to the different oxidising/wetting characters of the atmospheres, suggesting contribution of different species to the electrical transport. In wet O_2, the impedance spectrum shows a predominant arc for frequencies lower than 10^4 Hz with a prevalent capacitive contribution of 10^{-3} F, attributable to the polarisation processes at the electrodes. The electrolyte contribution to the overall transport is displayed as a shift of the spectrum in the real axis. Also, an inductive tail ascribed to the overall setup arises at higher frequencies. On the contrary, the spectrum under dry O_2 is dominated by a high frequency contribution ascribed to the transport through the electrolyte and a minor low-frequency arc associated to the electrode polarization process. These features point not only to a higher resistance under dry atmospheres, but also suggest a higher contribution to the overall conductivity from electronic species. Broadly speaking, similar behaviours are observed under N_2 atmospheres, with higher resistances of the electrolyte contribution in comparison to the O_2 atmospheres.

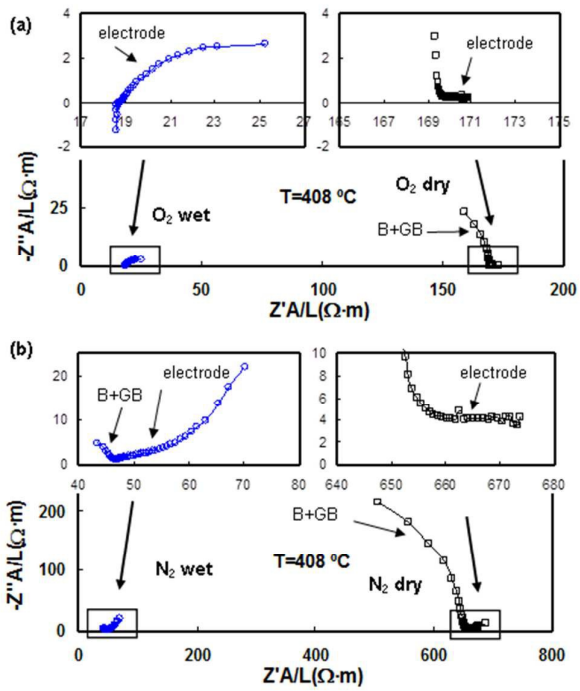

Figure. 3. Impedance spectra obtained at 408 °C under dry/wet conditions of O_2 (a) and N_2 (b).

View Article Online
DOI: 10.1039/C6TA02708C

In ceramic-protonic conductors, protons are incorporated in the lattice under wet conditions according to the hydration reaction: [2, 34]

$$H_2O + V_O^{\bullet\bullet} + O_O^X \Leftrightarrow 2OH_O^{\bullet} \quad (1)$$

where the equilibrium constant, K_w, could be approximated as:

$$K_W \approx \frac{[OH_O^{\bullet}]^2}{pH_2O.[V_O^{\bullet\bullet}]} \quad (2)$$

On the other hand, under oxidising conditions, the oxygen vacancies are also in equilibrium with electronic holes by means of the oxygen gaseous species according to:

$$\frac{1}{2}O_2 + V_O^{\bullet\bullet} \Leftrightarrow O_O^X + 2h^{\bullet} \quad (3)$$

The mass action law of Eq. 3 could be approximately expressed as:

$$K_O \approx \frac{[h^{\bullet}]^2}{pO_2^{1/2}.[V_O^{\bullet\bullet}]} \quad (4)$$

According to Eqs. 1-4, the concentration of oxygen vacancies, protons and holes is directly dependent on pO_2, pH_2O and T. The electroneutrality law for charged species in wet environments is expressed as follows:

$$2[S_B^{\bullet\bullet}] + 2[V_O^{\bullet\bullet}] + [OH_O^{\bullet}] + [h^{\bullet}] = [In_B'] \quad (5)$$

where the presence of In^{3+} and S^{6+} in the B position of the perovskite should be counterbalanced by the rest of charged defects.

The temperature dependence of conductivity under several gas conditions is shown in Fig. 4. The results in dry gases show an improvement in conductivity under the more oxidising character of O_2 gas in comparison to N_2 gas, which suggests that hole species affect the overall electrical transport, according to Eqs. 3-4. The activation energy is ~0.85 eV in the whole range of temperature for dry conditions of both O_2 and N_2, in agreement with that expected for this contribution [35]. Under humid atmospheres, an enhancement of conductivity is apparent between 350-550 ºC, in comparison to dry conditions, for both gases. This is a clear indication that protonic species are involved in the overall conduction. The activation energy in wet environments is ~0.34-0.39 eV, in the aforementioned temperature range. The measured value of activation energy is a consequence of the different conduction processes associated with the various species. In the current case its value points to protons as the prevalent carriers[2, 7, 10]. The measured activation energy rises for temperatures higher than 550 ºC and the values of conductivity approach those obtained under dry conditions. The exothermic enthalpy of Eq. 1 implies that the concentration of protons would decrease for higher temperatures[2]. This phenomenon supports the minor contribution of protonic species in this range, which leaves oxygen vacancies and electron holes as the main electrical carriers. The conductivity values offered by the $Ba_2In_{1.8}S_{0.2}O_{5+\delta}$material in Fig.4 are higher than that shown for the base $Ba_2In_2O_5$ material in the literature[10, 24], underscoring the beneficial nature of oxygen disorder upon sulfur(VI) doping.

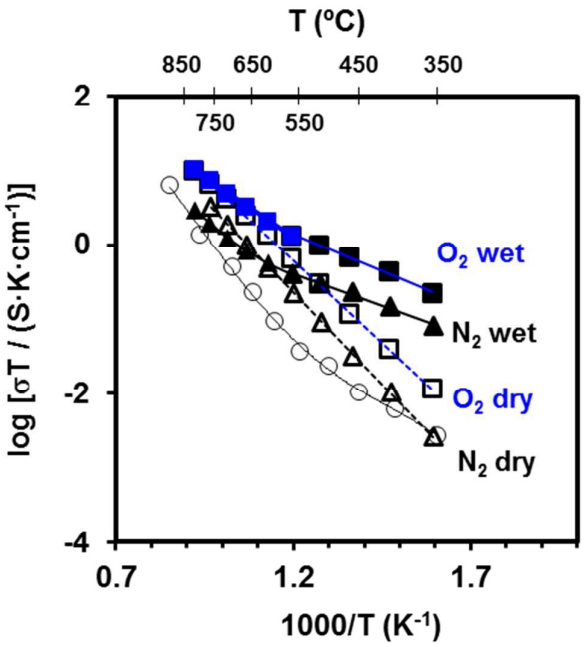

Figure. 4. Temperature dependence of conductivity in wet and dry conditions of N_2 and O_2. A value of $pH_2O \approx 0.023$ atm was employed under wet conditions. Open circles represent literature conductivity data of $Ba_2In_2O_5$ in wet air[10]

The specific conductivity of the various carriers under wet and dry conditions was obtained by means of a modified emf methodology in the range 500-800 °C.

For determination of the protonic conductivity under wet conditions, each side of the sample (sealed onto an YSZ tube) was submitted to the same N_2/O_2 mixture of 41.25/8.75 ml·min^{-1}/ml·min^{-1}, which produces the same value of $pO_2 \approx$ 0.175 atm in both compartments. Simultaneously, a gradient of pH_2O was established by exposing each gas flow to different levels of humidification controlled by mixing wet and dry gas fractions. A pH_2O ratio of ~5.75x10^{-3} / 2.3x10^{-3} atm/atm was selected during the experiment for this aim. Under these conditions, an auxiliary-variable resistance located in parallel to the sample produces a modification of the measured electromotive force of the system (E_M) according to[32, 33].

$$\left(E_{H_2O}.E_M^{-1}\right) - 1 = \left(R_H + R_\eta\right)R_M^{-1} + \left(R_e^{-1} + R_O^{-1}\right)\left(R_H + R_\eta\right) \quad (6)$$

View Article Online
DOI: 10.1039/C6TA02708C

where R_H, R_e and R_O correspond to protonic, electronic and oxide-ionic resistances, respectively; R_M is the auxiliary-variable resistance; R_η is the electrode-polarization resistance associated to the electrochemical reaction during the permeation process, and E_{H_2O} corresponds to the Nernst voltage associated to the present pH_2O gradient, determined by:

$$E_{H_2O} = -\frac{RT}{2F}\ln\left(\frac{pH_2O'}{pH_2O''}\right) \qquad (7)$$

Equation 6 shows that the factor $\left[\left(E_{H_2O}.E_M^{-1}\right)-1\right]$ presents a linear behaviour as a function of the variable R_M^{-1}. It follows that the protonic conductivity under the present working conditions can be determined by:

$$\sigma_H = \sigma_T - (\sigma_O + \sigma_e) = \left[R_T^{-1} - \left(R_O^{-1} + R_e^{-1}\right)\right]\frac{L}{A} \qquad (8)$$

where the factor $\left(R_O^{-1} + R_e^{-1}\right)$ is determined by the intercept over the slope of the linear representation of Eq. 6 and R_T is the total resistance of the sample, which is determined independently by impedance spectroscopy at the same working conditions.

For the determination of electronic and oxide-ionic conductivities, the average values of pO_2 and pH_2O were maintained as the same of the first experiment. In this situation, it is considered that the transport properties are imposed by the average working conditions through the sample. Therefore, a pO_2 gradient of 0.25/0.1 atm/atm was created across the sample by applying a mixture of 12.5 ml·min^{-1} of O_2 and 37.5 ml·min^{-1} of N_2 to one compartment and 5 ml·min^{-1} of O_2 with 45 ml·min^{-1} of N_2 to the other compartment. Both mixtures were hydrated to produce the same $pH_2O \approx 4.025\times10^{-3}$ atm in both chambers. The implementation of an external-variable resistance modifies the measured value of emf according to [33]:

$$\left(E_{O_2}.E_M^{-1}\right) - 1 = C.R_M^{-1} + C.R_e^{-1} \qquad (9)$$

Where C is a constant value that depends on the protonic resistance and oxide-ionic resistance of the sample and the polarisation resistance of the electrodes, and E_{O_2} is the Nernst voltage associated to the pO_2 gradient, according to:

$$E_{O_2} = \frac{RT}{4F}\ln\left(\frac{pO_2'}{pO_2''}\right) \qquad (10)$$

From Eq. 9 it follows that the value R_e^{-1} could be determined from the intercept over the slope of the linear representation of $\left[\left(E_{O_2}.E_M^{-1}\right)-1\right]$ vs. R_M^{-1}. Thus, the electronic- and oxide-ionic conductivities could be obtained according to the expressions presented below:

$$\sigma_e = R_e^{-1}\frac{L}{A} \qquad (11)$$

$$\sigma_O = \sigma_T - (\sigma_H + \sigma_e) = [R_T^{-1} - (R_H^{-1} + R_e^{-1})]\frac{L}{A}$$
$$= [(R_O^{-1} + R_e^{-1}) - R_e^{-1}]\frac{L}{A} \qquad (12)$$

Note that the values $\left(R_O^{-1} + R_e^{-1}\right)$ and R_e^{-1} are directly obtained from the described experiments.

Fig. 5 shows an example of the dependence of E_M as a function of R_M^{-1} at 650 °C under the pH_2O gradient and the constant pO_2 indicated above in the first experiment. A very good fit between the experimental data and a linear behaviour is apparent, supporting the methodology. The complementary experiment with a pO_2 gradient and constant pH_2O was then accomplished to determine the electrical conductivities associated to the various species. This procedure was repeated at each temperature in the range 500-800 °C, and the results are shown in Fig. 6 for dry and wet conditions. For dry conditions, a specific situation of the second experiment with a pO_2 gradient arises, where it is assumed that the material possesses an insignificant content of protonic species. Therefore, Eqs. 9-12 are also shown to be valid, with the particularity of $R_H^{-1} \approx 0$.

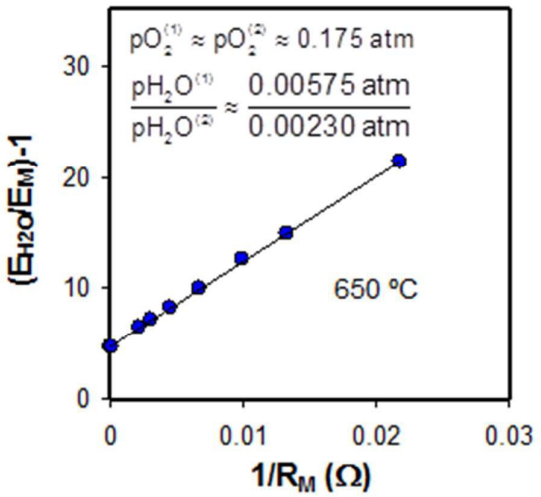

Figure 5. Linear dependence of the measured emf of the sample with the variable auxiliary resistance. Note that E_M is the measured value of emf, E_{H2O} is the Nernst value associated with the same gradient of pH_2O and R_M is the corresponding value of the auxiliary resistance that produces the modification of the experimental emf.

View Article Online
DOI: 10.1039/C6TA02708C

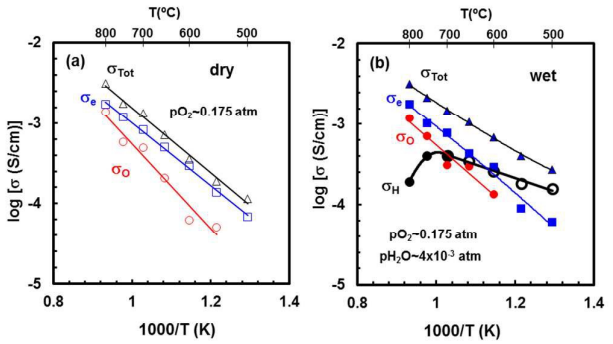

Figure 6. Temperature dependence of the conductivity associated to different species in dry (a) and wet (b) conditions.

Fig. 6(a) shows that the sample possesses a mixed oxide-ionic/electronic behaviour in dry conditions, due to the prevalent equilibrium between the oxygen vacancies and electron holes in oxidising atmospheres (Eq. 3). On the other hand, under humid atmospheres, a protonic component emerges, with a positive impact on the overall transport, mainly for temperatures lower than 700 °C, and governing the electrical conductivity for T ≤ 550 °C. The exothermic character of the hydration reaction (Eq. 1) reduces the concentration of protons as temperature rises, which leads to a maximum in protonic conductivity at about 700-750 °C, decreasing for higher temperatures, despite an improved mobility. As a consequence, the electrical conductivity is practically identical in both wet and dry atmospheres for T ≥ 800 °C (Figs. 4 and 6).

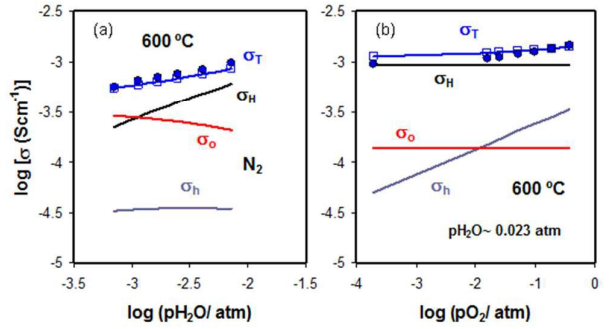

Figure 7. Experimental results of conductivity (closed circles) as a function of pH_2O in N_2 atmosphere (a) and as a function of pO_2 for a fixed value of $pH_2O \approx 0.023$ atm. Estimations of conductivity associated to different charge carriers (lines) are also presented.

The effect of working conditions on the transport properties was also analysed by changing the wet/dry dilution ratio and/or the oxidising character of the atmosphere. Fig. 7 shows the total conductivity obtained by impedance spectroscopy in a symmetric atmosphere of N_2 as a function of pH_2O (Fig. 7(a)) and as a function of pO_2, using wet mixtures of N_2/O_2, for a fixed value of $pH_2O \approx 0.023$ atm (Fig. 7(b)). The experimental results were contrasted with the estimated behaviour according to the defect chemistry. For this purpose, the concentration of protons and holes were expressed as a function of the oxygen vacancy concentration by means of Eqs. 2 and 4. This was combined with the electroneutrality law (Eq. 5), resulting in a 2-order-polynomial equation, which is analytically solved to obtain the concentration of the different species for the desired range of pO_2 and pH_2O (Fig. 8)[36] (note that the determination of pO_2 in N_2 atmosphere was performed by means of a YSZ-pO_2 sensor). Table 2 shows the values of equilibrium constants and mobility ratios between different carriers used to obtain the estimations of defect profiles and conductivities. Some values extracted from literature for other perovskite systems are also shown for comparison[37-41]. Fig. 8(a) shows that the concentration of holes as a function of pO_2 in wet N_2 is practically constant. We should note here that the use of N_2 produces a slight increase of pO_2 for higher pH_2O. This produces the effect that the hole-concentration profile is slightly altered in comparison to that which would be obtained for a fixed value of pO_2. A slight decrease in hole concentration should, thus, be obtained as pH_2O rises under these conditions. On the other hand, Fig. 8(a) shows that the concentration of ionic species is at least three orders of magnitude higher than that of electronic carriers, with predominance of oxygen vacancies in drier conditions and protons in wetter conditions. The increase of pO_2 in the latter situation has the effect to increase the concentration of holes with a 1/4 –power law dependence (Eq. 4), keeping both the concentration of protons and oxygen vacancies as constants (Fig. 8(b)). The introduction of the expected mobilities of the various carriers allows the fitting of experimental data with those obtained from the defect chemistry. Although the latter results are only estimations, they fit well with the experimental values. It is noteworthy that both graphs in Fig. 7 were fitted simultaneously with the same parameters (equilibrium constants and mobilities) to support the methodology.

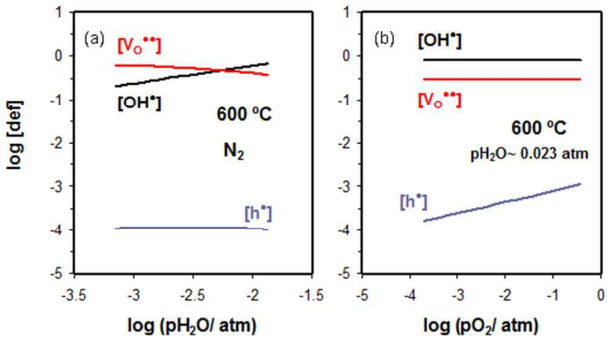

Figure 8. Estimations of defect profiles associated to different carriers, according to the defect chemistry, as a function of pH_2O in N_2 atmosphere (a) and as a function of pO_2 for mixtures of N_2/O_2 in wet conditions.

According to the literature (Table 2) it is expected that the mobility of protons is several times higher than that of oxygen vacancies and the hole mobility should be at least two orders of magnitude higher than that of ionic species. As a consequence, under N_2 atmosphere (Fig. 7(a)), the total conductivity seems not to be affected by electronic holes,

View Article Online
DOI: 10.1039/C6TA02708C

whereas protons dominate the overall transport at higher humidities and oxygen vacancies have some influence for drier conditions. Conversely, an increase in pO_2 at the highest humidities ($pH_2O \approx 0.023$ atm), produces a mixed-conducting behaviour with a raised contribution of the electronic component (Fig. 7(b)), despite its lower charge carrier concentration (Fig. 8(b)). These results highlight the possibility of tuning the mixed transport properties of the studied sulfur-doped $Ba_2In_2O_{5+\delta}$ material by selection of the appropriate environmental conditions, pointing to a wide range of possibilities in intermediate temperature electrochemical applications, such as the electrochemical promotion of chemical reactions[42, 43], membrane reactors[44] and also fuel cells[45].

Table 2. Equilibrium constants and mobility ratios between different charge carriers employed in the simulation of defect profiles and conductivities by means of the defect chemistry. Some values extracted from literature for other perovskite systems are also shown for comparison.

Compound	K_W (atm^{-1})	K_O ($atm^{-1/2}$)	μ_H/μ_O	μ_h/μ_H	Reference, T (°C)
$BaIn_{1.8}S_{0.2}O_{5+\delta}$	90	$7x10^{-6}$	5	$2.6x10^{2}$	This work, 600
$Ba_{0.97}Y_{0.03}Ce_{0.84}Y_{0.16}O_{2.935}$	~120				K.D. Kreuer et al [41], 600
$SrCe_{0.95}Yb_{0.05}O_{3-\delta}$	~50	$\sim 5x10^{-6}$	~20	$\sim 10^{2}$	F. Krug et al.[40], 600
$SrCe_{0.95}Yb_{0.05}O_{3-\delta}$		$\sim 8x10^{-6}$		$\sim 10^{2}$	H. Uchida et al.[38], 600
$AB_{1-y}M_yO_{3-y/2\pm\delta}$	20	10^{-5}			Bonanos et al [37], 800

4. Conclusions

A disordered orthorhombic perovskite was successfully synthesised by the introduction of a sulfur content of x=0.2 in $Ba_2In_{2-x}S_xO_{5+\delta}$. The overall electrical conductivity of the obtained composition is considerably enhanced in comparison to literature data on the undoped sample, related to the improved disorder of the oxygen sublattice. Different charge species were found as dominant electrical carriers on the variation of the environmental conditions such as temperature, oxygen partial pressure and water partial pressure. In dry oxidising atmospheres, the electrical behaviour is dominated by both oxide-ions and hole carriers, due to the equilibrium between oxygen vacancies and holes under conditions of high pO_2. Under humid environments the hydration reaction occurs and protonic species arise at the expense of oxygen vacancies. Protonic carriers control the overall electrical transport for temperatures lower than 550 °C, while having an insignificant contribution at temperatures higher than 750 °C. A mixed contribution from protons, oxide ions and holes is apparent between 550-700 °C, pointing to interesting applications for intermediate temperature devices, such as electrochemical membranes.

Acknowledgements

The authors acknowledge financial support from the FCT, POPH, PTDC/CTM/100412/2008, PTDC/CTM/105424/2008, FCT Investigator Programme, project IF/00280/2012, IF/01344/2014/CP1222/CT0001, QREN, FEDER and COMPETE Portugal and the European Social Fund, European Union. D. Pérez-Coll is acknowledged to the FCT for financial support by a BPD grant (SFRH/BPD/112282/2015).

References

1. J. B. Goodenough, *Annu. Rev. Mater. Res.*, 2003, **33**, 91-128.
2. K. D. Kreuer, *Annu. Rev. Mater. Res.*, 2003, **33**, 333-359.
3. H. Yokokawa, T. Horita, N. Sakai, K. Yamaji, M. E. Brito, Y. P. Xiong and H. Kishimoto, *Solid State Ionics*, 2004, **174**, 205-221.
4. J. Guan, S. E. Dorris, U. Balachandran and M. Liu, *Solid State Ionics*, 1997, **100**, 45-52.
5. E. D. Wachsman, C. A. Marlowe and K. T. Lee, *Energy Environ. Sci.*, 2012, **5**, 5498-5509.
6. A. J. Jacobson, *Chem. Mater.*, 2010, **22**, 660-674.
7. J. B. Goodenough, J. E. Ruiz-Diaz and Y. S. Zhen, *Solid State Ionics*, 1990, **44**, 21-31.
8. G. B. Zhang and D. M. Smyth, *Solid State Ionics*, 1995, **82**, 161-172.
9. N. Bonanos, *Solid State Ionics*, 1992, **53**, 967-974.
10. G. B. Zhang and D. M. Smyth, *Solid State Ionics*, 1995, **82**, 153-160.
11. C. A. J. Fisher and M. S. Islam, *Solid State Ionics*, 1999, **118**, 355-363.
12. T. Schober, J. Friedrich and F. Krug, *Solid State Ionics*, 1997, **99**, 9-13.
13. J. F. Q. Rey, F. F. Ferreira and E. N. S. Muccillo, *Solid State Ionics*, 2008, **179**, 1029-1031.
14. T. Hashimoto, Y. Inagaki, A. Kishi and M. Dokiya, *Solid State Ionics*, 2000, **128**, 227-231.
15. W. Fischer, G. Reck and T. Schober, *Solid State Ionics*, 1999, **116**, 211-215.
16. H. Yamamura, Y. Yamada, T. Mori and T. Atake, *Solid State Ionics*, 1998, **108**, 377-381.
17. T. Yao, Y. Uchimoto, M. Kinuhata, T. Inagaki and H. Yoshida, *Solid State Ionics*, 2000, **132**, 189-198.
18. K. Kakinuma, H. Yamamura, H. Haneda and T. Atake, *Solid State Ionics*, 2001, **140**, 301-306.
19. K. Kakinuma, H. Yamamura, H. Haneda and T. Atake, *J. Therm. Anal. Calorim.*, 1999, **57**, 737-743.
20. T. Q. Ta, T. Tsuji and Y. Yamamura, *J. Alloys Compd.*, 2006, **408–412**, 253-256.
21. C. A. J. D. Fisher, B.; Brook, R. J. , *Br. Ceram. Proc.*, 1996, **56**.
22. Y. K. Uchimoto, M. , *J. Appl. Phys.* , 1999, **38-1**
23. R. Hui, R. Maric, C. Decès-Petit, E. Styles, W. Qu, X. Zhang, J. Roller, S. Yick, D. Ghosh, K. Sakata and M. Kenji, *J. Power Sources*, 2006, **161**, 40-46.
24. J. F. Shin, L. Hussey, A. Orera and P. R. Slater, *Chem. Commun.*, 2010, **46**, 4613-4615.
25. J. F. Shin, A. Orera, D. C. Apperley and P. R. Slater, *J. Mater. Chem.*, 2011, **21**, 874-879.
26. J. F. Shin, D. C. Apperley and P. R. Slater, *Chem. Mater.*, 2010, **22**, 5945-5948.

View Article Online
DOI: 10.1039/C6TA02708C

27. J. F. Shin and P. R. Slater, *J. Power Sources*, 2011, **196**, 8539-8543.
28. A. M. R. Abakumov, Marta D. ; Gutnikova, Olga Yu.; Drozhzhin, Oleg A.; Leonova, Ludmila S.; Dobrovolsky, Yuri A.; Istomin, Sergey Ya. , *Chem. Mater.*, 2008, **20**, 10.
29. J. Rodríguez-Carvajal, *Physica B: Condensed Matter*, 1993, **192**, 55-69.
30. A. D. A. Brandao, I.; Frade, J. R.; Torre, J.; Kharton, V. V.; Fagg, D. P. , *Chem. Mater.* , 2010, **22**.
31. D. P. Sutija, T. Norby and P. Björnbom, *Solid State Ionics*, 1995, **77**, 167-174.
32. D. Perez-Coll, G. Heras-Juaristi, D. P. Fagg and G. C. Mather, *J. Mater. Chem. A*, 2015, **3**, 11098-11110.
33. D. Pérez-Coll, G. Heras-Juaristi, D. P. Fagg and G. C. Mather, *J. Power Sources*, 2014, **245**, 445-455.
34. A. S. Nowick and Y. Du, *Solid State Ionics*, 1995, **77**, 137-146.
35. S. Ricote, N. Bonanos, H. J. Wang and R. Haugsrud, *Solid State Ionics*, 2011, **185**, 11-17.
36. A. L. Chinelatto, K. Boulahya, D. Perez-Coll, U. Amador, C. Tabacaru, S. Nicholls, M. Hoelzel, D. C. Sinclair and G. C. Mather, *Dalton Trans.*, 2015, **44**, 7643-7653.
37. N. Bonanos and F. Willy Poulsen, *J. Mater. Chem.*, 1999, **9**, 431-434.
38. H. Uchida, H. Yoshikawa, T. Esaka, S. Ohtsu and H. Iwahara, *Solid State Ionics*, 1989, **36**, 89-95.
39. T. Schober, W. Schilling and H. Wenzl, *Solid State Ionics*, 1996, **86–88, Part 1**, 653-658.
40. F. Krug, T. Schober and T. Springer, *Solid State Ionics*, 1995, **81**, 111-118.
41. K. D. Kreuer, T. Dippel, Y. M. Baikov and J. Maier, *Solid State Ionics*, 1996, **86–88, Part 1**, 613-620.
42. B. Lee, Y. Sakamoto, D. Hirabayashi, K. Suzuki and T. Hibino, *J. Catal.*, 2010, **271**, 195-200.
43. I. Kalaitzidou, A. Katsaounis, T. Norby and C. G. Vayenas, *J. Catal.*, 2015, **331**, 98-109.
44. S. Hamakawa, T. Hibino and H. Iwahara, *J. Electrochem. Soc.*, 1994, **141**, 1720-1725.
45. M. Yano, A. Tomita, M. Sano and T. Hibino, *Solid State Ionics*, 2007, **177**, 3351-3359.

View Article Online
DOI: 10.1039/C6TA02708C

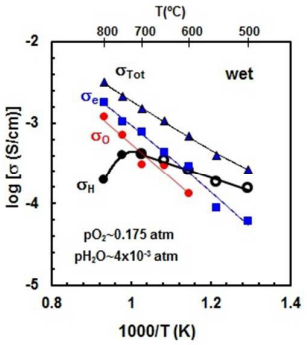

Temperature dependence of the conductivity of $Ba_2In_{1.8}S_{0.2}O_{5.3}$ associated to different species, protonic, σ_H, electronic, σ_e, and oxide-ionic, σ_o, in wet conditions.